Soft Matter

Accepted Manuscript

ROYAL SOCIETY OF CHEMISTRY

www.rsc.org/softmatter

Vesicle dynamics in uniform electric fields: squaring and breathing

Lane C. McConnell[a], **Petia M. Vlahovska**[*b] **and Michael J. Miksis**[*c]

Received Xth XXXXXXXXXX 20XX, Accepted Xth XXXXXXXXX 20XX
First published on the web Xth XXXXXXXXXX 200X
DOI: 10.1039/b000000x

We computationally investigate the dynamics of a vesicle exposed to uniform DC or AC electric fields. We employ the two-dimensional boundary integral method in order to simulate vesicle deformation under experimental conditions where peculiar drum-like ("squared") shapes have been observed. The vesicle membrane is modeled as an infinitely thin, capacitive, area-incompressible interface, with the surrounding fluids acting as leaky dielectrics. Our simulations capture the "squaring" phenomenon, in which vesicles deform into rectangular profiles with corner-like regions of high curvature, as vesicles undergo dynamic transitions between oblate and prolate ellipsoidal shapes.

1 Introduction

Electrodeformation of giant vesicles (cell-size sacs made of lipid or block-copolymer bilayers) is a classical approach to probe the electromechanical properties of biomimetic fluid membranes[1,2]. Elongation of a quasi–spherical vesicle in a uniform AC field is commonly used to measure bending rigidity[1,3]. The frequency-dependence of the vesicle asphericity, namely the transition between prolate and oblate spheroidal shapes, has been recently utilized to infer membrane capacitance[4]. The time-dependent dynamics of intact, non-porated vesicles in DC pulses yields information about membrane viscosity, as well as bending rigidity and tension[5]. Poration following DC pulses and pore closure serve to determine line tension[6]. Electric fields have also been used to modulate the phase transitions in tri-component membranes (made of neutral lipids), and found to decrease the miscibility temperature[7].

Interpretation of electrodeformation experiments relies on theoretical models[3,5,8–15]. These models, however, are limited to nearly spherical[3,5,8–12] or strictly spheroidal shapes[13–15], and cannot explain the peculiar drum-like shapes observed in the experiments with quasi-spherical vesicles[16]. Such drastic shape distortions can be captured only with numerical simulations. While vesicle dynamics in external flows has been extensively simulated[17–26], few papers have considered the effects of electric fields[27,28]. The electrohydrodynamics of vesicles is challenging computationally because one needs to consider both the evolution of the electric field and the fluid motion accompanying vesicle deformation. We have developed a computational approach based on the Boundary Integral Method in two dimensions to simulate vesicle responses to electric and flow fields[27]. Our previous paper was devoted to the development of the numerical method and provided only few illustrative examples of vesicle electrohydrodynamics in the case of DC field and fast bulk conduction. In this paper, we apply our numerical method to comprehensively study vesicle dynamics to DC and AC fields and map vesicle responses on phase-diagrams of relevant physical parameters.

2 Model

The vesicle is neutrally-buoyant and filled with an electrolyte solution with viscosity μ_{in}, permittivity ε_{in}, and conductivity σ_{in}. It is suspended in a second electrolyte solution with different viscosity μ_{ex}, permittivity ε_{ex}, and conductivity σ_{ex}. The contrast in physical properties of the bulk fluids is characterized by the ratios

$$\eta = \frac{\mu_{in}}{\mu_{ex}}, \quad \xi = \frac{\varepsilon_{in}}{\varepsilon_{ex}}, \quad \Lambda = \frac{\sigma_{in}}{\sigma_{ex}}. \tag{1}$$

Vesicle deflation is quantified by its reduced area $\Delta = A/(\pi a^2)$, where A is its area (2D volume), L is its perimeter, and $a = L/(2\pi)$ is the radius of a circle with the same perimeter (2D area). A value of $\Delta = 1$ indicates a perfect circle, while smaller values indicate increasingly deflated shapes. Throughout our calculations we use a as the characteristic length scale and set the dimensionless perimeter to be $L = 1$.

The lipid bilayer membrane is assumed to have no net charge, and to be of uniform conductivity σ_m and dielectric permittivity ε_m. In the zero–thickness model of the membrane, these properties yield an effective surface capacitance $C_m = \varepsilon_m/h$ and conductivity $G_m = \sigma_m/h$, where h is the membrane thickness (typically $h \sim 5nm$.)

[a] *Department of Math and Statistics, University of New Mexico, Albuquerque, NM 87131, USA. Tel: ++1 505 2772114; E-mail: lmcconne@math.unm.edu*
[b] *School of Engineering, Brown University, Providence, RI 02912, USA.*
[c] *Engineering Sciences and Applied Mathematics, Northwestern University, Evanston, IL 60208, USA.*

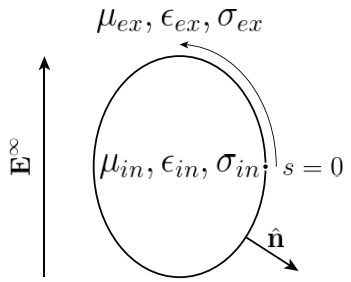

Fig. 1 Sketch of the problem: an initially elliptical vesicle placed in a uniform electric field. The interface is parametrized in terms of arclength s measured from the vesicle equator.

The molecular thickness of the bilayer gives rise to resistance to bending; the simplest relation between surface stresses and changes in curvature is described by the Helfrich model[29,30]. Moreover, the total number of lipid molecules in each monolayer is conserved, which renders the membrane virtually inextensible and gives rise to nonuniform tension (2D pressure). The membrane stresses are given by[31,32]

$$\boldsymbol{\tau}^m = -\kappa(H_{ss} + H^3/2)\mathbf{n} - (\Sigma \mathbf{x}_s)_s\,, \tag{2}$$

where $\mathbf{x} = \mathbf{x}(s,t)$ is the position of the vesicle membrane as a function of arclength s and time t, $\hat{\mathbf{n}}$ is the outward pointing normal to the membrane, κ is the bending modulus, H is the mean curvature, and Σ is the membrane tension. The subscript s denotes a derivative with respect to arclength. As a result of the membrane's area–inextensibility, the tension is not a material parameter, but a Lagrange multiplier enforcing the inextensibility condition, i.e., zero surface-divergence of the interfacial velocity.

The vesicle is placed in a uniform electric field $\mathbf{E}^{\infty}$ (see Figure 1) with magnitude E_0

$$\mathbf{E}^{\infty} = E_0 f(t)\hat{\mathbf{y}}\,, \tag{3}$$

where $f(t)$ describes any time dependence, e.g., in an AC field, $f(t) = \sin(2\pi\omega t)$. The vesicle dynamics in the electric field are described within the framework of the leaky–dielectric model which consists of Ohm's law for the electric current and Stokes equations for fluid motion, see Saville[33] for a derivation from the Poisson-Nernst-Planck equations. Accordingly, the electric field is irrotational, $\mathbf{E} = -\nabla\phi$, and the electric potential satisfies the Laplace's equation

$$\nabla^2\phi_k = 0, \quad k = in, ex. \tag{4}$$

The interfacial capacitance leads to a jump of the electric potential at the interface $V_m = \phi_{in} - \phi_{ex}$. This transmembrane potential, V_m, is calculated from the conservation of electrical current in the normal direction[34,35]

$$\sigma_{ex}E_n^{ex} - G_m V_m = C_m\frac{DV_m}{Dt} - \varepsilon_{ex}\frac{DE_n^{ex}}{Dt} \tag{5a}$$

$$\sigma_{in}E_n^{in} - G_m V_m = C_m\frac{DV_m}{Dt} - \varepsilon_{in}\frac{DE_n^{in}}{Dt}\,, \tag{5b}$$

where $D/Dt = \frac{\partial}{\partial t} + \mathbf{v}\cdot\nabla$ is the material derivative along the interface and E_n^{in} and E_n^{ex} are the normal components of the electric field on the interior and exterior of the membrane, respectively. The electric potential and field are determined from Eq.(4) subject to the boundary conditions Eq.(3) and Eq.(5). The electric forces acting on the membrane can then be determined from the jump in the Maxwell stresses across the membrane given by

$$\boldsymbol{\tau}^{el} = \mathbf{n}\cdot(\mathbf{T}_{ex}^{el} - \mathbf{T}_{in}^{el})\,, \tag{6}$$

where $\mathbf{T}^{el} = \varepsilon(\mathbf{EE} - \frac{1}{2}\mathbf{E}\cdot\mathbf{EI})$.

Vesicle deformation is determined from the kinematic condition for the position of the interface,

$$\frac{d\mathbf{x}}{dt} = \mathbf{v}_{ex} = \mathbf{v}_{in} \tag{7}$$

which simply matches the velocity of the interface, $d\mathbf{x}/dt$, to the velocities of the fluid on either side of the interface, $\mathbf{v}_{ex}$ and $\mathbf{v}_{in}$. This formulation treats the membrane as a water-impermeable surface which, coupled with the incompressibility of the fluid, ensures that the volume of the vesicle is conserved.

The fluid velocity $\mathbf{v}$ is a solution of the Stokes equations (since the fluid motion at the scale of the micron-sized vesicle is dominated by viscous effects and inertia is negligible)

$$\mu_k\nabla^2\mathbf{v}_k - \nabla p_k = 0, \quad \nabla\cdot\mathbf{v}_k = 0. \tag{8}$$

where p is the fluid pressure. The forces due to fluid motion acting on the membrane are computed from the jump in the hydrodynamic stress tensor across the interface

$$\boldsymbol{\tau}^{hd} = \mathbf{n}\cdot(\mathbf{T}_{ex}^{hd} - \mathbf{T}_{in}^{hd}) \tag{9}$$

where $T_{ij}^{hd} = -\delta_{ij}p + \mu(\frac{\partial \mathrm{v}_i}{\partial x_j} + \frac{\partial \mathrm{v}_j}{\partial x_i})$. To solve for the flow, one needs one more boundary condition. It is provided by the condition for mechanical equilibrium at the interface, which requires that the shape-distorting hydrodynamic and electric stresses, Eq.(6) and Eq.(9), are balanced by the shape-preserving membrane elastic stresses, Eq.(2)

$$\boldsymbol{\tau}^{hd} + \boldsymbol{\tau}^{el} = \boldsymbol{\tau}^{m}\,. \tag{10}$$

Henceforth we nondimensionalize all variables using the vesicle radius a as the characteristic length scale and a time scale set by the charging of the membrane capacitor $t_m = aC_m/\sigma_{ex}$. Accordingly, the characteristic stress is $\tau_c = \mu_{ex}/t_m$. The scaling introduces several dimensionless parameters: membrane conductivity $G = aG_m/\sigma_{ex}$, field strength $\beta = \varepsilon_{ex}E_0^2/\tau_c$, bending rigidity $\chi = \kappa/a^3\tau_c = C_m\kappa/\sigma_{ex}\mu_{ex}a^2$,

Table 1 Dimensionless parameters: definitions and typical range

Dimensionless parameter	Description	Range of values
$\beta \equiv \varepsilon_{ex} E_0^2 a C_m / \mu_{ex} \sigma_{ex}$	electric field strength	10^{-4} to 10^{2}
$\chi \equiv C_m \kappa / \sigma_{ex} \mu_{ex} a^2$	bending rigidity	10^{-4} to 10^{-3}
$G \equiv a G_m / \sigma_{ex}$	membrane conductivity	≈ 0 for intact bilayer
$\alpha \equiv \varepsilon_{ex} / a C_m$	bulk charge relaxation time	10^{-3}
$\Lambda \equiv \sigma_{in} / \sigma_{ex}$	conductivity ratio	10^{-2} to 10
$\eta \equiv \mu_{in} / \mu_{ex}$	viscosity ratio	10^{-1} to 10^{1} (typically near 1)
$\xi \equiv \varepsilon_{in} / \varepsilon_{ex}$	dielectric permittivity ratio	typically near 1
$\Omega \equiv \omega a C_m / \sigma_{ex}$	AC field frequency	0 to 100

charge relaxation time in the bulk $\alpha = \varepsilon_{ex}/aC_m$, and dimensionless AC field frequency $\Omega = \omega a C_m/\sigma_{ex}$. The dimensionless parameters and their typical values in experiments are listed in Table 1. The estimates are based on the typical values from experiments[5,16,36–39]: vesicle radius $a \approx 10\mu m$, electric field strength $E_0 \approx 1 - 100 kV/m$, membrane bending modulus $\kappa \approx 10^{-19} J$, bulk fluid viscosity $\mu_{ex} \approx 10^{-3} Pa \cdot s$, permittivity $\varepsilon_{ex} \approx 10^{-10} F/m$, and conductivity $\sigma_{ex} \approx 10^{-4} S/m$. For pure, intact lipid membranes $G_m \approx 0$ because the membrane is impermeable to ions. Membrane conductivity becomes significant in the presence of ion channels or pores, and its values can vary widely.

3 Summary of the computational method

While small deformations of a nearly–spherical vesicle allow analytical solutions, large deformations are tractable only by numerical simulations. Here we outline our approach[27]. The boundary integral method utilizes potential theory and the divergence theorem to transform the equations of electric potential Eq.(4) and fluid velocity Eq.(8) from partial differential equations over the entire domain to line integrals along the vesicle interface, thereby reducing computational complexity. As the equations for the fluid velocity, Stokes' equations can be reformulated into boundary integral form as

$$\frac{1+\eta}{2} v_i(\mathbf{x}_0) = v_i^{\infty}(\mathbf{x}_0) - \int_0^L \frac{1}{4\pi} G_{ij}^{hd}(\mathbf{x},\mathbf{x}_0) f_j(\mathbf{x}) ds + \int_0^L \frac{1-\eta}{4\pi} T_{ijk}^{hd}(\mathbf{x},\mathbf{x}_0) v_j(\mathbf{x}) n_k(\mathbf{x}) ds \quad (11)$$

where $G_{ij}^{hd}(\mathbf{x},\mathbf{x}_0) = -\delta_{ij} \ln r + \hat{x}_i \hat{x}_j / r^2$ is the two-dimensional Stokeslet, $T_{ijk}^{hd} = -4\hat{x}_i\hat{x}_j\hat{x}_k/r^4$ is the stresslet, and f_j is the sum of all interfacial forces. In these expressions $\hat{\mathbf{x}} = \mathbf{x} - \mathbf{x}_0$ and $r = |\hat{\mathbf{x}}|$ is the distance between $\mathbf{x}_0$ and $\mathbf{x}$, another point on the interface[40].

Following a similar procedure, the equations for the electric potential at a point $\mathbf{x}_0$ either inside or outside the vesicle are given in boundary integral form by

$$\phi_{in}(\mathbf{x}_0) = 2\int_0^L \Big(G^{el}(\mathbf{x},\mathbf{x}_0) \nabla \phi_{in} - \phi_{in} \nabla G^{el}(\mathbf{x},\mathbf{x}_0) \Big) \cdot \mathbf{n} ds \quad (12a)$$

$$\phi_{ex}(\mathbf{x}_0) = 2\phi^{\infty}(\mathbf{x}_0) - 2\int_0^L \Big(G^{el}(\mathbf{x},\mathbf{x}_0) \nabla \phi_{ex} - \phi_{ex} \nabla G^{el}(\mathbf{x},\mathbf{x}_0) \Big) \cdot \mathbf{n} ds \quad (12b)$$

where $G^{el}(\mathbf{x},\mathbf{x}_0) = -\ln r/2\pi$ is the free space Green's function for the Laplace equation, $\nabla G^{el}(\mathbf{x},\mathbf{x}_0) = -(\hat{\mathbf{x}} \cdot \mathbf{n})/2\pi r^2$ is its gradient, and $\hat{\mathbf{x}}$ and r are defined as previously. Introducing $V_m = \phi_{in} - \phi_{ex}$ and $U_m = \phi_{in} + \phi_{ex}$, we can add and subtract Eq.(12a) and Eq.(12b) to get

$$V_m(\mathbf{x}_0) = -2\phi^{\infty}(\mathbf{x}_0) - 2\int_0^L \Big((E_n^{in}(\mathbf{x}) + E_n^{ex}(\mathbf{x})) G^{el}(\mathbf{x},\mathbf{x}_0) + U_m \nabla G^{el}(\mathbf{x},\mathbf{x}_0) \Big) \cdot \mathbf{n} ds \quad (13a)$$

$$U_m(\mathbf{x}_0) = 2\phi^{\infty}(\mathbf{x}_0) - 2\int_0^L \Big((E_n^{in}(\mathbf{x}) - E_n^{ex}(\mathbf{x})) G^{el}(\mathbf{x},\mathbf{x}_0) + V_m \nabla G^{el}(\mathbf{x},\mathbf{x}_0) \Big) \cdot \mathbf{n} ds. \quad (13b)$$

This equation must be solved subject to the current continuity equation at the interface Eq.(5), which in dimensionless form is

$$\frac{DV_m}{Dt} + G V_m = E_n^{ex} + \alpha \frac{DE_n^{ex}}{Dt} = \Lambda E_n^{in} + \xi \alpha \frac{DE_n^{in}}{Dt}. \quad (14)$$

The other drivers of the vesicle dynamics are the elastic membrane forces and the electric forces, which appear in the term f_j in Eq.(11). These forces are derived from the stress balance defined in Eq.(10), and are given in dimensionless form by

$$\mathbf{f} = \chi \left(\mathbf{x}_{ssss} - (\Sigma \mathbf{x}_s)_s - \beta \| E_i E_j - \delta_{ij} E^2/2 \| n_i \right) \quad (15)$$

where $\| E_i E_j - \delta_{ij} E^2/2 \| = (E_i^{in} E_j^{in} - \delta_{ij} E^{in^2}/2) - \xi (E_i^{ex} E_j^{ex} - \delta_{ij} E^{ex2}/2)$ represents the jump in the Maxwell stress at the interface.

The equations of fluid motion Eq.(11) and electric potential Eq.(13) have a complicated, nonlinear interdependence. The electric field at the interface depends on the vesicle shape, and the vesicle shape, in turn, depends on the forces derived from the electric field. Further complicating matters is the innate computational stiffness of the fluid equations (due to the dependence of the membrane force on fourth–order derivative terms), which gives explicit solution methods dramatically restrictive stability conditions. To circumvent this issue, we employ a semi-implicit, second-order backwards difference scheme[41] which allows for accurate and stable solutions of the equations.

In each of our simulations, the initial profile of the vesicle is an ellipse centered at the origin with its major axis aligned vertically (in the same direction as the imposed electric field). Theoretically, the fact that the shape of the vesicle, the electric field, and the forces acting on the vesicle are all symmetric should keep the vesicle dynamics symmetric for all time as well. Unfortunately, in some cases computer round-off error introduces enough small asymmetry to destabilize the dynamics and lead to non-physical, asymmetric results. To prevent this from happening, we actively enforce a two-fold symmetry on the vesicle at each timestep so that its shape remains identical from left to right and top to bottom for all times. To do so, the computations from the first quadrant are reflected across both axes to get the full vesicle shape. This preserves all symmetry in vesicle shape, fluid flow, and electric field that should theoretically be present.

The deformations are characterized by the aspect ratio ν, which compares the lengths of the vesicle contour parallel and perpendicular to the applied field. Using this definition, a vesicle has two primary shapes of interest. In three-dimensions, prolate ellipsoids (resembling hot dogs) are characterized by having one long major axis and two identical, smaller, minor axes. Oblate (hamburger shaped) ellipsoids are characterized by having one short minor axis and two identical, larger, major axes. In general, vesicles are often characterized using this same terminology for convenience despite the fact that they are not, generally speaking, perfectly ellipsoidal. In the context of this 2D study, values of $\nu > 1$ correspond to prolate shapes, while values of $\nu < 1$ correspond to oblate shapes.

4 Results

Next we present a parametric study of vesicle behaviors in DC and AC uniform electric fields. Unless otherwise noted, $\xi = 1$, $\eta = 1$, $\chi = 0.0005$, and $\Delta = 0.9$. We explore the effects of conductivity ratio Λ, field strength β, bulk charge relaxation α, membrane conductivity G, and AC field frequency Ω.

4.1 DC electric field: oblate-prolate transition and squaring

For a DC electric field, $f(t) = H(t)$ is the step function (uniformly 0 for $t \leq 0$ and uniformly 1 for $t > 0$).

Analytical theory[12] and experiments[5] have shown that a vesicle with $\Lambda/\xi < 1$ may initially deform into an oblate spheroid but eventually becomes a prolate spheroid (note that the excess area needed for the ellipsoidal deformation of a quasi-spherical vesicle comes from the ironing of thermal shape undulations. Our simulations do not consider shape fluctuations, hence the initial vesicle shape needs to be elliptical). In the context of our simulations, a vertically oriented elliptical vesicle ($\nu > 1$) transitions to a horizontally extended oblate state ($\nu < 1$) and then back into a prolate ($\nu > 1$)(POP transition). Figure 2 illustrates the shape evolution and the POP transition for a vesicle with $\Lambda/\xi < 1$ upon application of a uniform DC field.

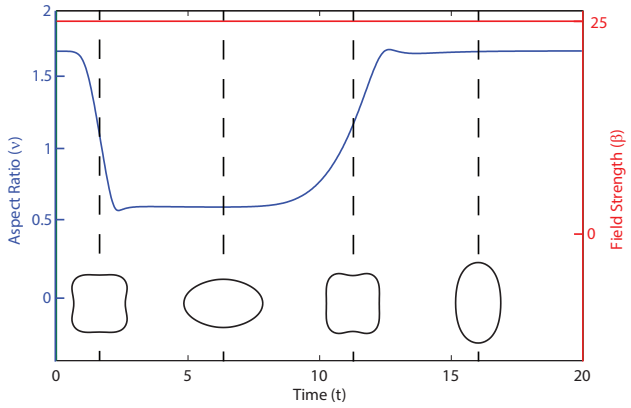

Fig. 2 Vesicle deformation upon application of a uniform DC field with strength $\beta = 25$. Conductivity ratio is $\Lambda = 0.1$, membrane conductivity $G = 0$, and bulk conduction is fast ($\alpha = 0$). The blue line denotes the aspect ratio ν of the vesicle; snapshots of vesicle contours are also shown. The red line shows the strength of the applied electric field β.

The transition depends strongly on the field strength and the mismatch in fluids conductivity and permittivity. Figure 3 shows that the POP transition can occur only if $\Lambda/\xi < 1$ and for a sufficiently strong electric field. Upon application of the electric field, the vesicle begins as a prolate ellipse. The electric field initially induces vertically compressive forces which act to squeeze the vesicle into an oblate profile. Over time, as the membrane charges, these compressional forces shift from vertical to horizontal, eventually causing the vesicle to elongate into a prolate shape where it remains indefinitely at its equilibrium orientation. This is the typical POP transition. However, the higher the excess area, the stronger the compression forces required to make the vesicle oblate. If the ver-

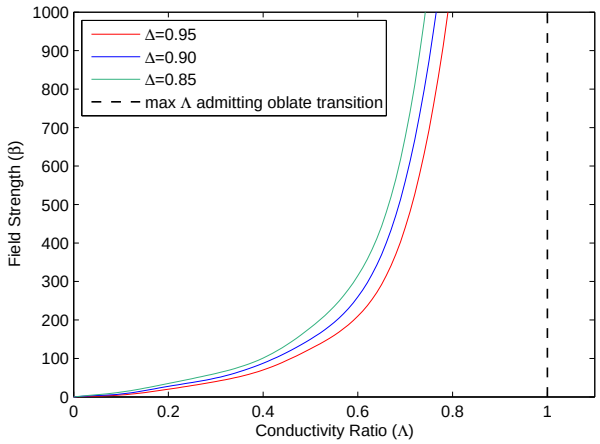

Fig. 3 The critical electric field strength β_c required to induce the POP transition increases with conductivity ratio Λ and vesicle deflation. $G = 0$ and $\alpha = 0$.

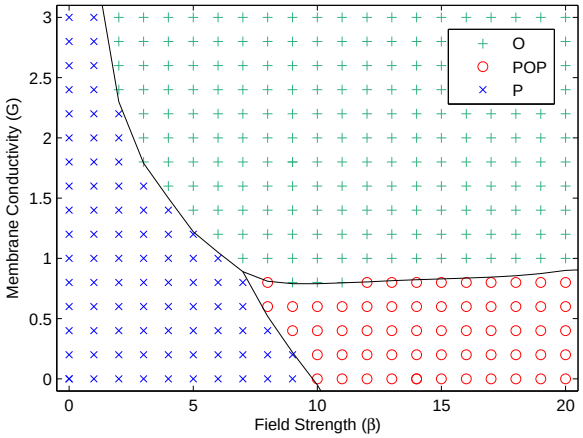

Fig. 4 The behavior of the vesicle as a function of the electric field strength β and membrane conductivity G. The vesicle either remains prolate (P) for all time, undergoes the prolate-oblate-prolate (POP) transition, or adopts steady oblate profile (O). $\Lambda = 0.1$ and $\alpha = 0$

tically compressive forces experienced by the vesicle are not strong enough, the vesicle compresses only slightly, remaining in a prolate state ($\nu > 1$), before approaching the equilibrium shape. Consequently, a full POP transition is not observed.

Another factor affecting the POP transition is the membrane conductivity. While increasing the membrane capacitance only increases the time scale of the charging, membrane conductance not only shortens the charging time but also reduces the transmembrane voltage. If $V_m = 0$ then the electric field at equilibrium is not expelled from the vesicle interior, and the vesicle experiences only oblate steady deformation for $\Lambda/\xi < 1$. Thus the effect of the membrane conductance is not only to suppress the POP transition, but also to create a range of field strengths in which the vesicle remains an oblate at equilibrium, see Figure 4. Membrane conductivity range is chosen based on Sens and Isambert[42].

The POP transition is also suppressed if charge relaxation in the bulk or charge convection along the interface are important, i.e., α is non-negligible. Similar behavior is reported for drops, where charge convection decreases oblate deformations[43,44]. Figure 5 demonstrates that the critical strength of the electric field β required to induce the POP dynamics on the vesicle increases with α.

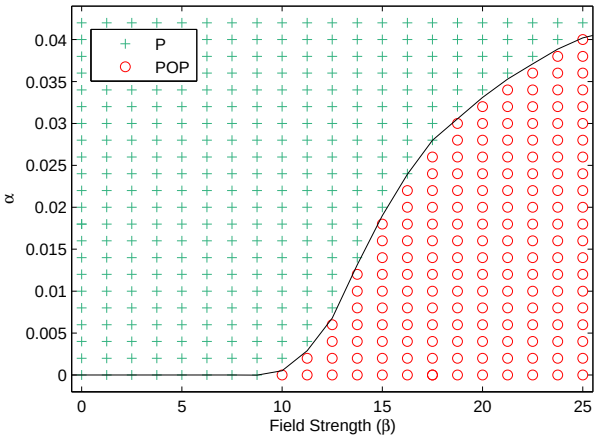

Fig. 5 Vesicle behavior as a function of the electric field strength β and charge relaxation in the bulk α. There are two behavior regimes: one in which prolate to oblate to prolate (POP) shape transitions occur, and one in which the vesicle remains prolate for all time (P). $\Lambda = 0.1$ and $G = 0$.

4.2 AC field: breathing

For an AC electric field, $f(t) = \sin(2\pi\Omega t)$ the vesicle dynamics become frequency-dependent, see Figure 6. In qualitative agreement with the experiments[45], vesicles are steady prolates at low frequencies, $\Omega \ll 1$, and steady oblates at higher frequencies, $\Omega \gg 1$. A new feature is predicted in strong fields and low frequencies, see Figure 7. Under the same conditions, in a DC field the vesicle remains in a prolate configuration at all times ($\beta < \beta_c$), while in the AC field, the vesicle undergoes "breathing" (vesicle shape oscillates between prolate and oblate shape). Since the electric stresses responsible for vesicle deformation are quadratic in field strength, the vesicle undergoes elongation-compression cycle twice per one period of the field oscillations, i.e., vesicle deformation oscillates with twice the frequency of the applied field. Note however, that the strong fields in this regime are likely to induce poration

before breathing dynamics can be observed experimentally. A modified AC field profile analogous to the DC pulse profile used in Salipante and Vlahovska[5] may circumvent this issue.

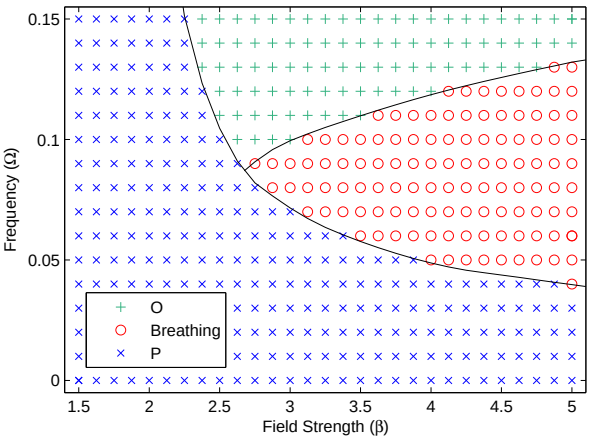

Fig. 6 Vesicle dynamics as a function of field strength and AC frequency. $\Lambda = 0.1$ and $\alpha = 0$.

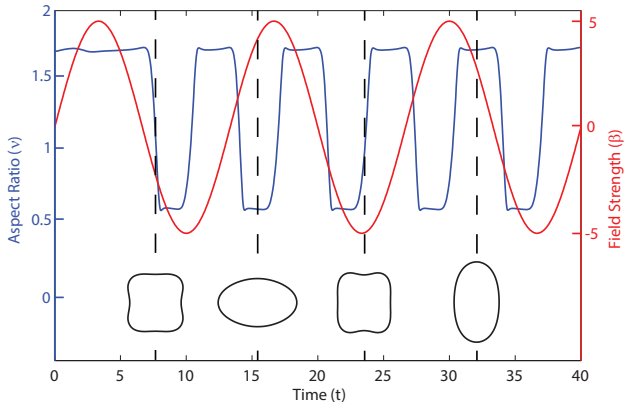

Fig. 7 The shape evolution of a vesicle in a AC field with strength $\beta = 5$ and frequency $\Omega = 0.075$. $\Lambda = 0.1$ and $\alpha = 0$. The line in blue shows the time evolution of the aspect ratio ν of the vesicle, while the red line shows the corresponding electric field strength β at that time.

4.3 Electroporation

Poration due to electric fields is of great practical and fundamental interest[46,47]. While our computational methodology does not allow us to simulate the actual pore formation because it involves topological changes in the vesicle structure, there is insight to be gained about electroporation from our simulations. Opening of pores in the membrane is related to the electric field induced tension[37,48]. Areas of high tension are associated with regions of the membrane where the combined effect of the external forces is to pull the lipid molecules of the membrane apart, while areas of high negative tension are associated with regions of the membrane where the lipid molecules are being compressed. Accordingly, one might expect pores to form exclusively in regions of high tension and not in regions of low or negative tension. For instance, consider a vesicle undergoing the POP transition mentioned previously. Initially, the highest tension is at the poles (see Figure 8.a) and a prolate-shaped vesicle may porate there[14] if the tension is higher than the lysis tension[37]. If the field strength is insufficient to cause poration initially, as the vesicle "squares" the location of the highest tension shifts toward the corners (see Figure 8.c) and the high curvature edges can become the sites of poration[16].

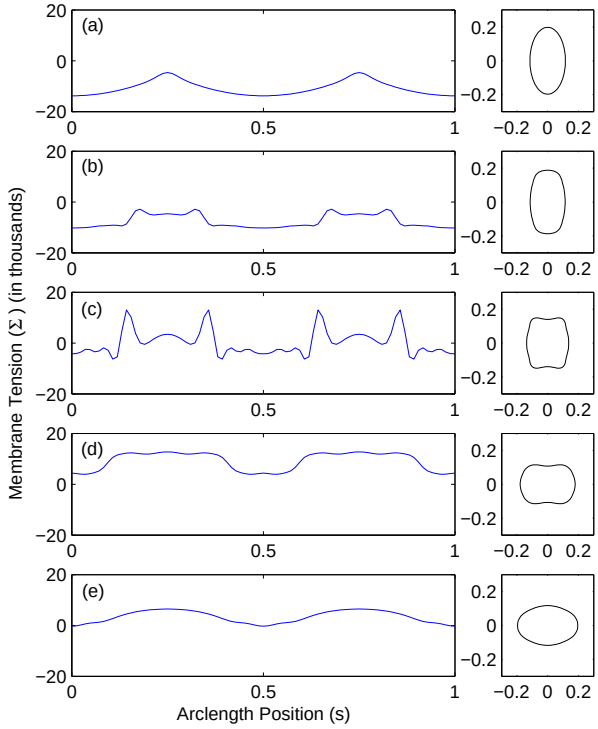

Fig. 8 A vesicle exposed to a DC electric field of strength $\beta = 25$. The membrane tension, Σ, is plotted as a function of arclength, s, along with the vesicle profile at times (a) $t/t_m = 0$, (b) 0.1, (c) 0.17, (d) 0.22, and (e) 0.6. The maximum tension occurs in the corner regions of (c) during vesicle squaring while transitioning between prolate and oblate states. $\Lambda = 0.1$, $G = 0$, and $\alpha = 0$.

5 Conclusions

We computationally studied vesicle dynamics in electric fields. Upon application of a uniform DC field, an initially prolate vesicle deforms into an oblate but eventually adopts a prolate shape. Our study shows that this prolate–oblate–prolate transition is possible only if $\Lambda/\xi < 1$, and it is sensitive to field strength, vesicle deflation, membrane conductivity, charge relaxation in the bulk and charge convection along the interface. During the prolate-oblate transition the vesicle can form corners and become "square". The corners are the locations of highest tension. An AC field evokes richer dynamics: in the case $\Lambda/\xi < 1$, a vesicle deforms into either an oblate spheroid for high AC frequencies, a prolate spheroid for low AC frequencies, or oscillates ("breathes") between the two states at intermediate AC frequencies. Our simulations also quantify tension variations along the membrane thereby suggesting potential sites for poration. Our work provides insights into the dynamics and stability of biomembranes in electric fields.

6 Acknowledgements

LCM was supported by NSF award DMS-1148801, PMV was partially supported by NSF awards CBET-1117099 and CMMI-1232477, and MJM by NSF award DMS-1312935.

References

1 R. S. Gracia, N. Bezlyepkina, R. L. Knorr, R. L. Lipowsky and R. Dimova, Soft Matter, 2010, **6**, 1472 – 1482.
2 H. Aranda-Espinoza, D. Hammer and D. Discher, Phys. Rev. Lett., 2001, **87**, 208301.
3 M. Kummrow and W. Helfrich, Phys. Rev. A, 1991, **44**, 8356–8360.
4 P. F. Salipante, R. Knorr, R. Dimova and P. M. Vlahovska, Soft Matter, 2012, **8**, 3810– 3816.
5 P. F. Salipante and P. M. Vlahovska, Soft Matter, 2014, **10**, 3386 –3393.
6 T. Portet and R. Dimova, Biophys. Journal, 2010, **99**, 3264–3273.
7 P. F. Salipante, M. L. Shapiro and P. M. Vlahovska, Procedia IUTAM, 2015, accepted.
8 M. Winterhalter and W. Helfrich, J. Phys. Chem., 1988, **92**, 6865.
9 P. M. Vlahovska, R. S. Gracia, S. Aranda-Espinoza and R. Dimova, Biophys. J., 2009, **96**, 4789–4803.
10 T. Yamamoto, S. Aranda-Espinoza, R. Dimova and R. Lipowsky, Langmuir, 2010, **26**, 12390–12407.
11 P. M. Vlahovska, in Advances in Planar Lipid Bilayers and Liposomes, vol. 12, ed. A. Iglic, Elsevier, 2010, pp. 103–146.
12 J. Schwalbe, P. M. Vlahovska and M. Miksis, Phys. Rev E, 2011, **83**, 046309.
13 J. Zhang, J. D. Zahn, W. Tan and H. Lin, Phys. Fluids, 2013, **25**, 071903.
14 M. M. Sadik, J. B. Li, J. W. Shan, D. I. Shreiber and H. Lin, Phys. Rev. E., 2011, **83**, 066316.
15 H. Nganguia and Y. N. Young, Phys. Rev. E, 2013, **88**, 052718.
16 K. A. Riske and R. Dimova, Biophys. J., 2006, **91**, 1778–1786.
17 S. K. Veerapaneni, D. Gueyffier, D. Zorin and G. Biros, J. Comp. Physics., 2009, **228**, 2334–2353.
18 S. K. Veerapaneni, A. Rahimian, G. Biros and D. Zorin, J. Comp. Phys., 2011, **230**, 5610–5634.
19 D. Salac and M. Miksis, J. Comp. Phys., 2011, **230**, 8192–8215.
20 D. Salac and M. Miksis, J. Fluid Mech., 2012, **711**, 122–146.
21 X. Li, P. M. Vlahovska and G. E. Karniadakis, Soft Matter, 2012, **9**, 28–37.
22 H. Noguchi and G. Gompper, Phys. Rev. Lett., 2004, **93**, 258102.
23 T. Biben, K. Kassner and C. Misbah, Phys. Rev. E, 2005, **72**, 041921.
24 T. Biben, A. Farutin and C. Misbah, Phys. Rev. E, 2011, **83**, 031921.
25 G. Boedec, M. Leonetti and M. Jaeger, J. Comput. Phys., 2011, **230**, 1020–1034.
26 J. Sohn, Y. Tseng, S. Li, A. Voigt and J. Lowengrub, J. Comp. Phys., 2010, **229**, 119–144.
27 L. McConnell, M. Miksis and P. Vlahovska, IMA J. Appl. Math., 2013, **78**, 797–817.
28 E. M. Kolandouz and D. Salac, Applied Mathematics Letters, 2015, **39**, 7–12.
29 W. Helfrich, Z. Naturforsch., 1973, **28c**, 693–703.
30 U. Seifert, Eur. Phys. J. B, 1999, **8**, 405–415.
31 S. K. Veerapaneni, R. Raj, G. Biros and P. K. Purohit, Int. J. Non-linear Mech., 2009, **44**, 257–262.
32 R. Finken, A. Lamura, U. Seifert and G. Gompper, Eur. Phys. J. E, 2008, **25**, 309–321.
33 D. A. Saville, Annu. Rev.Fluid Mech., 1997, **29**, 27–64.
34 K. DeBruin and W. Krassowska, Biophys. J., 1999, **77**, 1213–1224.
35 J. Seiwert and P. M. Vlahovska, Phys. Rev. E, 2012, **87**, 022713.
36 K. A. Riske and R. Dimova, Biophys. J., 2005, **88**, 1143–1155.
37 R. Dimova, K. A. Riske, S. Aranda, N. Bezlyepkina, R. L. Knorr and R. Lipowsky, Soft matter, 2007, **3**, 817–827.
38 R. Dimova, N. Bezlyepkina, M. D. Jordo, R. L. Knorr, K. A. Riske, M. Staykova, P. M. Vlahovska, T. Yamamoto, P. Yang and R. Lipowsky, Soft Matter, 2009, **5**, 3201 – 3212.
39 T. Portet, C. Mauroy, V. Demery, T. Houles, J.-M. Escoffre, D. S. Dean and M.-P. Rols, J. Membrane Biology, 2012, **245**, 555–564.
40 C. Pozrikidis, Boundary Integral and Singularity Methods for Linearized Viscous Flow, Cambridge University Press, 1992.
41 S. Veerapaneni, D. Gueyffier, G. Biros and D. Zorin, J. Comp. Phys., 2009, **228**, 7233–7249.
42 P. Sens and H. Isambert, Phys. Rev. Lett., 2002, **88**, Art. No. 128102.
43 J. Feng, Proc. Royal Soc. A, 1999, **455**, 2245–2269.
44 V. Y. Shkadov and A. A. Shutov, Fluid Dynamics, 2002, **37**, 713–724.
45 S. Aranda, K. A. Riske, R. Lipowsky and R. Dimova, Biophys. J., 2008, **95**, L19–L21.
46 R. Dimova, in Advances in Electrochemical Science and Engineering: Bioelectrochemistry, ed. R. Alkire, D. M. Kolb and J. Lipkowski, Wiley-VCH, Weinheim, 2011, pp. 335–367.
47 D. Miklavcic, B. Mali, B. Kos, R. Heller and G. Sersa, BIOMEDICAL ENGINEERING ONLINE, 2014, **13**, year.
48 D. Needham and R. M. Hochmuth, Biophys. J., 1989, **55**, 1001–1009.